J Mater Sci (2010) 45:3957–3960
DOI 10.1007/s10853-010-4545-x

LETTER

# Thermomechanical experiment and analysis on shape recovery properties of shape memory polymer influenced by fiber reinforcement

**M. Nishikawa · K. Wakatsuki · N. Takeda**

Received: 13 February 2010 / Accepted: 20 April 2010 / Published online: 4 May 2010


Shape memory polymers (SMPs) are currently investigated as potential materials for large deployable space structures [1–3]. The thermomechanical properties of these polymers significantly change on reaching their glass transition temperature, which yields the excellent feature of shape fixity and shape recovery [4]. As another aspect, the modulus of these materials is not sufficient since they are polymeric materials. In actual applications, the fiber reinforcement is effective for ensuring the sustainability of the deployed structures.

However, while the fiber reinforcement has advantages for increasing the stiffness, it has a negative influence on the shape recovery behavior of SMPs. Experimental studies for shape memory polymer composite were conducted by Gall et al. [5, 6] for SiC powder-reinforced nanocomposite, Ohki et al. [7] for short-glass-fiber reinforcement, and Lan et al. [8] for SMP reinforced with plain-weave fabrics, and the increase of residual strain after shape recovery process was confirmed. In order to maximize both the stiffness and shape-recovery behavior of fiber-reinforced SMPs, it is essential to know how the fibers block the shape recovery behavior of polymers. However, the mechanism was not modeled. Therefore, we focus on the mechanism underlying the degradation of shape recovery behavior due to fiber reinforcement.

To investigate this mechanism, we first conducted thermomechanical cycle tests for pure SMP and SMP reinforced with short-carbon fibers. We used polyurethane series of thermoset SMP, Diary MP-5510 (curing temperature 100 °C), provided by SMP Technologies Inc. The cured polymer has a glass transition temperature of 55 °C, and the temperature range of glass transition between glassy state and rubbery state is 30 °C. Short carbon fibers T700S (Toray Industries Inc.) were embedded in the polymer. The fibers with approximately 5 mm length were randomly embedded in the prepolymer before curing, and the weight fraction of fibers was set to 0, 2, and 4 wt%. It should be noted that the bundle of carbon fibers (12,000 fibers) was embedded and not dispersed in these model experiments, as also modeled later. After curing, strip specimens were cut out (approximately 40 mm gauge length, 20 mm width, and 2 mm thickness in average).

The following thermomechanical cycle was applied to these specimens using a tensile test machine (INSTRON 5566), as shown in Fig. 1:

(a) Tension at 75 °C until a predetermined maximum strain (8%) by 1%/min strain rate
(b) Cooling to 35 °C by −3 K/min cooling rate at constant strain
(c) Unloading at 35 °C by −0.1%/min strain rate
(d) Heating to 75 °C by 3 K/min while zero stress was kept.

The test fixture was set in a temperature-controlled bath, and the temperature was measured with a thermocouple attached to the specimen.

Figure 2 presents the results of thermomechanical cycle tests for pure SMP and SMP with carbon fibers. In these

M. Nishikawa (✉)
Department of Nanomechanics, Tohoku University,
6-6-01 Aoba-yama, Aoba-ku, Sendai 980-8579, Japan
e-mail: nishikawa@mm.mech.tohoku.ac.jp

K. Wakatsuki
Department of Aeronautics and Astronautics, The University of Tokyo, 5-1-5 Kashiwanoha, Kashiwa-shi, Chiba, 277-8561, Japan

N. Takeda
Department of Advanced Energy, The University of Tokyo, 5-1-5 Kashiwanoha, Kashiwa-shi, Chiba, 277-8561, Japan

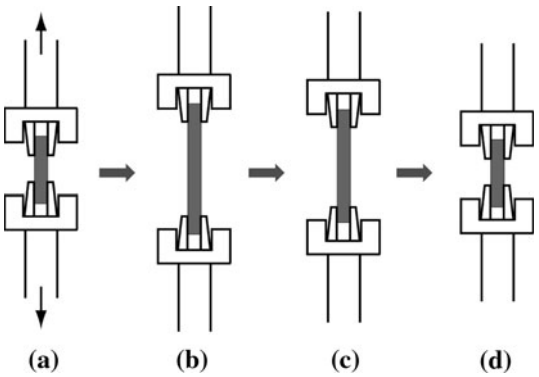


**Fig. 1** Schematic of thermomechanical experiment. **a** Tension at 75 °C. **b** Cooling to 35 °C at constant strain (shape fixity). **c** Unloading at 35 °C. **d** Heating to 75 °C at zero stress (shape recovery)

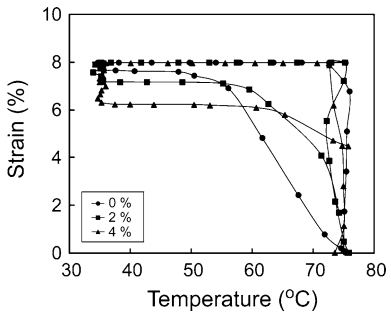


**Fig. 2** Experimental result on the influence of the thermomechanical behavior of SMP due to fiber reinforcement (0, 2 and 4 wt% carbon fibers)

results, the plots of experimental data are periodically sampled, because the temperature data fluctuated in these experiments. The shape recovery speed decreased with increasing weight fraction of carbon fibers. As a consequence, the residual strain after the thermomechanical cycle increased for SMP with carbon fibers. The applied strain was almost eliminated by the shape recovery process in the case of pure SMP, while the shape recovery was not completed for SMP with 4 wt% carbon fibers and the residual strain was about 4.5% due to fiber reinforcement (0, 2, and 4 wt% carbon fibers)

To discuss these experimental results, we present a thermomechanical finite element analysis to model the shape-recovery process in SMP with carbon fibers. We constructed a plane-strain finite element model for an SMP with 4 wt% carbon fibers, as shown in Fig. 3, and analyzed its thermomechanical behavior during a thermomechanical cycle. Based on the procedure described in our previous literature [9], we created a micromechanical model consisting of randomly arranged fibers and SMP. The fiber volume fraction $V_f$ was set to 2.5% (which corresponds to 4 wt%). In the experiments, the fiber was not individually

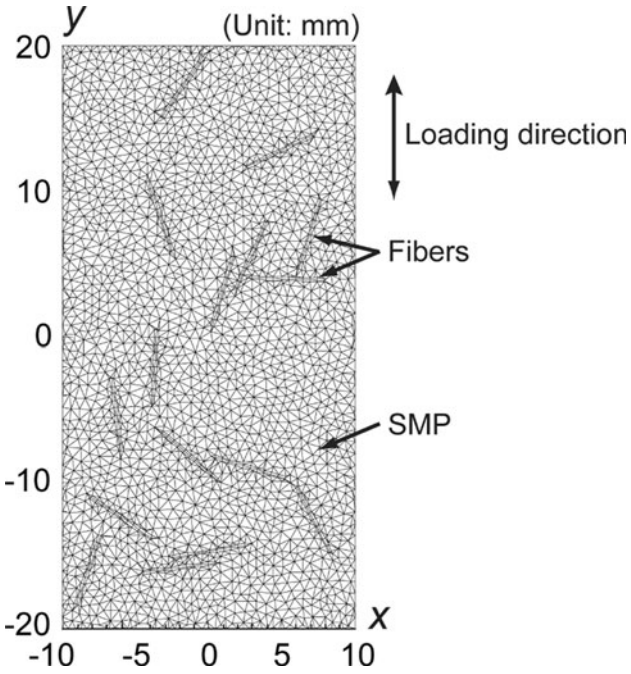


**Fig. 3** Finite element model of SMP with carbon fibers

dispersed in the specimen, but a bundle of fibers was condensed together. Thus, we modeled a carbon fiber as a rectangular region with 5 mm length × 0.25 mm width.

The fiber was divided into 9-node isoparametric quadrilateral elements while the SMP region was divided into 6-node triangle elements. The carbon fiber was modeled as orthotropic elastic body. The material properties of the fiber were set to $E_1 = 232$ MPa, $E_2 = E_3 = 14$ GPa as Young's modulus, $\nu_{12} = \nu_{13} = 0.2$, $\nu_{23} = 0.35$ as Poisson's ratio, $G_{12} = G_{13} = 20$ GPa, $G_{23} = 10$ GPa as elastic shear modulus. The thermal expansion coefficient of the fiber was set to $\alpha_1 = -0.38 \times 10^{-6}$ K$^{-1}$, $\alpha_2 = \alpha_3 = 26 \times 10^{-6}$ K$^{-1}$.

The present finite element analysis incorporated the constitutive relationship of SMP proposed by Tobushi et al. [10, 11]. The model is based on the theory of linear viscoelastic solid [12]. Here we assumed that the thermomechanical properties of the polymer are isotropic and all normal components behave in the same constitutive rule. This model relates the stress, $\sigma$, and strain, $\varepsilon$, considering elastic strain, stress relaxation process, creep process, and thermal strain, as follows:

$$\dot{\varepsilon} = \frac{\dot{\sigma}}{E} + \frac{\sigma}{\mu} - \frac{\varepsilon - \varepsilon_s}{\lambda} + \alpha\dot{T} \tag{1}$$

where $E$, $\mu$, $\lambda$, and $\alpha$ denote elastic modulus, viscosity coefficient, retardation time, and thermal expansion coefficient, respectively.

One important feature of the model is that it addresses the irrecoverable creep strain, $\varepsilon_s$, in Eq. 1. Tobushi et al.

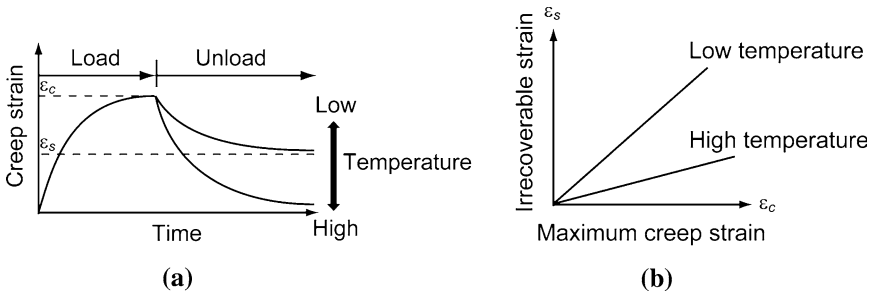


**Fig. 4** Schematic of the irrecoverable creep strain which depends on the temperature and maximum creep strain as investigated by Tobushi et al. [10]. **a** Schematic of irrecoverable creep strain. **b** Dependence on maximum creep strain

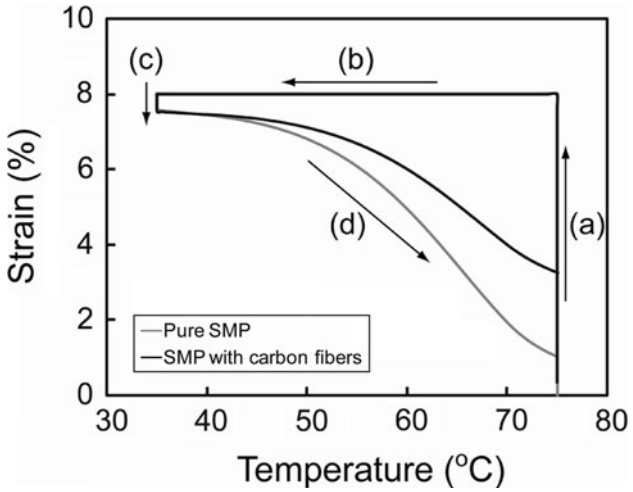


**Fig. 5** Comparison of the simulated results between pure SMP and SMP with carbon fibers

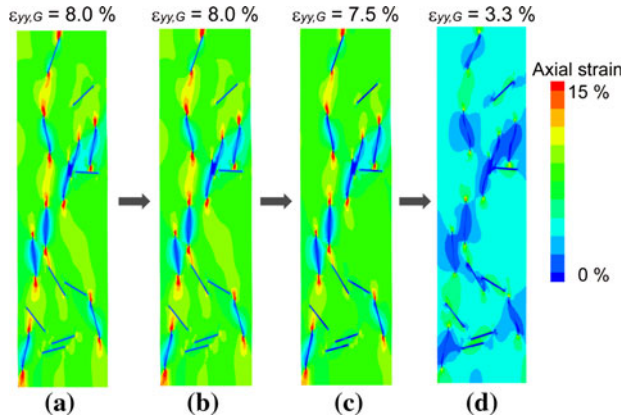


**Fig. 6** Strain-recovery distribution obtained with the simulation for SMP with carbon fibers. **a** Tension at 75 °C. **b** Cooling to 35 °C at constant strain (shape fixity). **c** Unloading at 35 °C. **d** Heating to 75 °C at zero stress (shape recovery)

investigated the irrecoverable creep strain of polyurethane SMP using creep tests, and they revealed that the irrecoverable creep strain depends on temperature and the maximum creep strain during loading as well, as schematically illustrated in Fig. 4. Thus, their model relates the irrecoverable strain, $\varepsilon_s$, to the creep strain, $\varepsilon_c$, which is calculated subtracting the elastic strain and thermal strain from the total strain, by the following linear function:

$$\varepsilon_s = S\varepsilon_c \tag{2}$$

where $S$ is a proportional constant. In addition, the material parameters $x$ ($E$, $\mu$, $\lambda$, and $S$) depend on the temperature, $T$, within the temperature range of glass transition between glassy state and rubbery state, as below.

$$x = x_g \exp\left\{a\left(\frac{T_g}{T} - 1\right)\right\} \tag{3}$$

where $x_g$ denotes the value at glass transition temperature $T_g$.

The material parameters were obtained by fitting with the experimental results for pure SMP, because the SMP material used in the present study was slightly different from that used by Tobushi et al. Here, three material parameters ($E$, $\mu$, $\lambda$) are important for the behavior of SMP during a thermomechanical cycle. Therefore, we fitted these three parameters, and we set other parameters to the values reported by Tobushi et al. [11]. These parameters at $T_g$ are as follows: $E = 32.1$ MPa, $\mu = 5.23 \times 10^3$ GPa s, $\lambda = 5.85 \times 10^2$ s, $\alpha = 1.16 \times 10^{-4}$ K$^{-1}$, $S = 0.1$, and $a = 38$.

Using the finite element model, we reproduced a thermomechanical cycle in experiments. Leaving both side edges of the model to be free edges, we controlled global tensile strain $\varepsilon_{yy,G}$ of the model (as described in [9, 13, 14]). The applied thermomechanical cycle was the same as the experimental cycle (steps (a)–(d) in Fig. 1). The time step in the analysis was set to $\Delta t = 20$ s for the steps (a)–(c) and $\Delta t = 2$ s for step (d). In step (d), we controlled zero stress by adjusting the global tensile strain increment so that the next tensile stress was expected to become zero, using Crank–Nicholson method.

Figure 5 presents the simulated results for SMP with 4 wt% carbon fibers. In this analysis, the maximum strain during a thermomechanical cycle was set to 8%. In the figure, we also present the analytical results for pure SMP obtained with the thermomechanical model given by Eq. 1. The tendency that the residual strain after a thermomechanical cycle increases due to fiber reinforcement is similar to the experimental results.

Figure 6 shows the tensile strain distribution in the SMP with carbon fibers obtained with the simulation for a thermomechanical cycle. These figures were obtained just after each step (step (a)–(d)) of a thermomechanical cycle. Just after the loading step (step (a): Fig. 6a), the strain concentrates in the vicinity of fiber ends. Although the global maximum strain was set to 8% strain, the maximum strain was well above 15% strain. Thus, the local irrecoverable strain becomes large due to Eq. 2 (Fig. 4b), and the residual strain after the thermomechanical cycle increases as a result of the strain concentration near fiber ends, as shown in Fig. 6d. Then the simulated results in Fig. 5 show that the residual strain becomes large for SMP with carbon fibers. Moreover, as mentioned by Tobushi et al., the increase of the irrecoverable strain reduces the shape-recovery speed as well (Fig. 4a). For these reasons, the fiber reinforcement brings about the degradation of shape-recovery behavior (i.e. shape recovery speed and residual strain).

From these discussions, we can conclude that the local irrecoverable strain becomes large in the region where SMP is subjected to a large deformation by the existence of short fiber ends. Therefore, in order to quantify the irrecoverable strain and discuss the shape recovery behavior in these SMP composites, it is essential to model the microstructure consisting of fiber and SMP and investigate the local strain concentration on SMP.

## References


1. Ishizawa J, Imagawa K, Yoshikawa J, Hayashi S, Miwa N (2001) In: Proceedings of SAMPE JAPAN 2001
2. Ishizawa J, Shimamura H, Minami S, Imagawa K, Hayashi N, Miwa N, Hayashi S (2005) In: Proceedings of IAC 2005, IAC-05-C2.4
3. Lin JKH, Knoll CF, Willey CE (2006) AIAA 2006-1896
4. Lendlein A, Kelch S (2002) Angew Chem Int Ed 41:2034
5. Gall K, Dunn ML, Liu Y, Finch D, Lake M, Munshi N (2002) Acta Mater 50:5115
6. Liu Y, Gall K, Dunn ML, McCluskey P (2004) Mech Mater 36:924
7. Ohki T, Ni QQ, Ohsako N, Iwamoto M (2004) Composites A 35:1065
8. Lan X, Liu Y, Lv H, Wang X, Leng J, Du S (2009) Smart Mater Struct 18:024002
9. Nishikawa M, Okabe T, Takeda N (2009) J Solid Mech Mater Eng 3:998
10. Tobushi H, Hayashi S, Ito N, Takata T (2000) Trans Jpn Soc Mech Eng A 64:502 (in Japanese)
11. Tobushi H, Okumura K, Hayashi S, Ito N (2001) Mech Mater 33:545
12. Lockett FJ (1972) Nonlinear viscoelastic solids. Academic Press, London
13. Nishikawa M, Okabe T, Takeda N (2009) Adv Compos Mater 18:77
14. Nishikawa M, Okabe T (2010) Int J Solid Struct 47:398